

# We are IntechOpen, the world's leading publisher of Open Access books Built by scientists, for scientists

6,900

Open access books available

186,000

International authors and editors

200M

Downloads

Our authors are among the

154

Countries delivered to

TOP 1%

most cited scientists

12.2%

Contributors from top 500 universities



WEB OF SCIENCE™

Selection of our books indexed in the Book Citation Index  
in Web of Science™ Core Collection (BKCI)

Interested in publishing with us?  
Contact [book.department@intechopen.com](mailto:book.department@intechopen.com)

Numbers displayed above are based on latest data collected.  
For more information visit [www.intechopen.com](http://www.intechopen.com)



---

# Fabrication of TiO<sub>2</sub> Nanoparticles and Thin Films by Ultrasonic Spray Pyrolysis: Design and Optimization

---

Raymond Taziwa and Edson Meyer

Additional information is available at the end of the chapter

<http://dx.doi.org/10.5772/67866>

---

## Abstract

Ultrasonic spray pyrolysis (USP) methods offer an economical, efficient, and dependable method of depositing nanoparticles (NPs) with consistent crystalline structure and stoichiometry. The need for precise control of structural, morphological, and optical properties has stimulated researches on development spray pyrolysis (SP) methods for depositing titanium dioxide nanoparticles (NPs) and thin films (TF) to substitute traditional sophisticated and expensive wet chemistry methods and solid state techniques. SP methods, as compared to other solid state techniques, offer precise control of the stoichiometry of precursor's solutions prepared by wet chemistry methods. Moreover, SP methods offer deposition simplicity as the NPs and TFs are deposited at room temperature and pressure. The deposited NPs and TFs are produced in a single-step route without the need for laborious, expensive purification and excessive annealing procedures. The present chapter offers the experimental challenges and accomplishments experienced while working with the USP systems. Knowledge gathered was key to the development of the present USP system presented herein. This book chapter starts by presenting a review of the current methods available for fabrication of TiO<sub>2</sub> NPs and TFs. This chapter also provides a detailed report on the numerous experimental considerations utilized in the optimization of the novel USP system for depositing titanium dioxide NPs and TFs. Finally, the design of the USP system is presented.

**Keywords:** aerosol process, ultrasonic spray pyrolysis, TiO<sub>2</sub>, nanopowders, thin films

---

## 1. Introduction

Nanostructures of titanium dioxide (TiO<sub>2</sub>) such as nanoparticle (NPs) and thin films (TFs) have over the past century received widespread attention [1]. For both research applications and industrial applications, TiO<sub>2</sub> has received wide attention due to its common applications as an

---

anode electrode for solar cells and anode electrode for photocatalytic degradation of organic waste [1, 2]. Notably,  $\text{TiO}_2$  displays exceptional opto-electronic properties. Moreover,  $\text{TiO}_2$  in addition to being a low-cost, wide band semiconductor material has unique chemical properties and is non-poisonous. Moreover, there are numerous stimuli for studying development of  $\text{TiO}_2$  NPs and TFs for solar applications.  $\text{TiO}_2$  TFs and NPs are currently employed as anode electrodes for solar cells. Moreover, the current industries involved in production of  $\text{TiO}_2$  NPs and TFs are accustomed with the technology and will not be hesitant to adapt to synthesis techniques. Furthermore, the necessary deposition equipment is operating today in the plants. As a consequence, the development of new solar cell technology that incorporates  $\text{TiO}_2$ -processing stages could be readily implemented by the current industry without the typical long lead in time for new technology.  $\text{TiO}_2$  NPs and TFs have been deposited by many different techniques, including the hydrothermal method [2], chemical vapor deposition [3], electrodeposition [4], pyrolysis [5], sol-gel method [6], spin methods [7], laser ablation [8], ion-assisted deposition [9], and spray pyrolysis methods [10, 11].

The structural, optical, electronic, and morphological properties of  $\text{TiO}_2$  NPs are closely dependent on the NPs physical properties such as size and stoichiometric composition; it is necessary to have a deposition technique in which these properties are easy to deal with. Moreover, the morphology, crystalline structure, structural properties, optical properties, electronic properties, and stoichiometry of  $\text{TiO}_2$  NPs and TFs have very sensitive deposition conditions. This is an inherent disadvantage for many physical vapor deposition methods [3, 7] such as laser ablation, where there are large variations in the optical and structural properties of the synthesized NPs and TFs [8]. These variations in NPs properties arise from small changes in the deposition conditions which are a key challenge in the development of techniques for the production of  $\text{TiO}_2$  NPs and TFs at a large industrial scale. Therefore, the need for stoichiometric techniques in  $\text{TiO}_2$  NPs and TFs suggests that a deposition method where the stoichiometry of the final product is controlled by a chemical reaction would enable more consistent results. Thus, much devotion has been dedicated on deposition of  $\text{TiO}_2$  NPs and TFs in a nano-scale range with consistent crystalline structure, morphology, and chemical stoichiometric ratios of  $\text{TiO}_2$ . Spray pyrolysis methods have proven to be reliable as they are able to control the stoichiometry precursor solutions by pyrolysis by utilizing a chemical reaction to control the chemical composition of the precursor solution [5, 10, 11]. Moreover, it is an inherent requirement when developing new methods for production of  $\text{TiO}_2$  NPs and TFs to keep the deposition system as simple as possible and keep costs at a minimum and, at the same time, maximize throughput. Spray pyrolysis methods offer such an opportunity. Moreover, in spray pyrolysis (SP) methods, NPs and TFs are produced in a one-step process without the need for further purification or excessive drying procedures, which has a negative effect on the total thermal budget and cost of production of  $\text{TiO}_2$  [13–15]. Equally, the technique can be used to coat large substrates and presents the opportunity for industrial scaling. Spray pyrolysis method, unlike other solid state deposition methods, presents a very simple reasonable economical method for depositing  $\text{TiO}_2$  NPs and TFs on industrial scale.

In SP methods, the precursor is produced via a precisely controlled chemical reaction to produce  $\text{TiO}_2$  and succeeds either by hydrolysis or pyrolysis. In hydrolysis, for SP-assisted systems, separate gas line of carrier gas is bubbled through heated baths of a liquid  $\text{TiO}_2$

precursor and water [13, 14]. The two delivery lines are then brought together close to the substrate where the reaction takes place. Hydrolysis systems have the advantage of simplicity; although, they may be relatively inflexible, as tubing diameters have to be designed around predicted flow rates. Pyrolysis systems are similar, except that a water bath is not required as the TiO<sub>2</sub> precursor decomposes upon reaching the heated substrate. To keep the deposition system as simple as possible, maximize throughput, and keep costs at a minimum, systems with a vacuum chamber were not considered to be a viable option. This excluded evaporation, sputtering, and the majority of chemical vapor deposition (CVD) systems. Spin-on methods were not seriously considered, as the throughput of any such system would be limited in a production environment. Screen-printing is commonly used in the photovoltaic industry PV industry for depositing metallic contacts, about 30–50 μm. Screen-printing has been used for depositing TiO<sub>2</sub> TFs [16, 17]. As the thickness of the metallic contacts is about 500 times thicker than the TiO<sub>2</sub> TFs, it is not known how the thinner films behaved with regard to reproducibility, squeegee wear, and thickness uniformity. Following the screen-printing of organometallic ink, the samples were fired in a three-step process for a 30 min duration [16, 17]. The firing is a relatively slow process as first; the thick film needs to settle for 15 min to obtain a uniform film, with subsequent drying performed at 125°C for 5 min. The final crystallization was performed in a belt furnace at temperatures between 500 and 900°C. Lengthy drying procedures are required to remove the substantial amount of organic solvents added to the TiO<sub>2</sub> precursor [18–21]. Therefore, to lower the thermal budget and processing costs, it would be attractive to deposit a nano-crystalline TiO<sub>2</sub> thin film in one step without subsequent heat treatment steps. Hence, in this book chapter, we present a novel, less-sophisticated, and economical ultrasonic spray pyrolysis (USP) system for production of high-quality TiO<sub>2</sub> NPs and TFs and design considerations of an ultrasonic spray pyrolysis system.

### 1.1. Experimental encounters with spray pyrolysis system

This section lays out practical experiences that the author's experienced while working with spray pyrolysis systems. The experience and knowledge gathered while working with SP systems played a pivotal role in designing, assembly, and optimization of the present SP system. Moreover, the knowledge gathered also helped shape the various considerations in selecting the equipment (reactor type, nebulizer size, ultrasonic vessel type, and furnace type) of the present SP system design. Furthermore, consideration is given to various material properties and deposition conditions that were used to optimize the design and construction of the present USP system. This section lays out practical huddles experienced with previous spray pyrolysis, more specifically for the production of TiO<sub>2</sub> NPs and TFs.

#### 1.1.1. Use of titanium tetrachloride precursor

The previous hybrid pneumatic/ultrasonic spray pyrolysis that the author worked with consisted of (1) tube furnace, (2) pneumatic nebulizer, and (3) quartz tube reactor as the reaction zone. Spray deposition was done on glass substrates lying horizontally inside the quartz tube reactor. In the study, titanium tetrachloride was employed as the precursor. The system also employed argon gas as the carrier gas in case the ultrasonic nebulizers were used. There were

a number of problems that existed with regard to deposition of  $\text{TiO}_2$  NPs and TFs. Firstly, the use of titanium tetrachloride as a precursor for synthesis of  $\text{TiO}_2$  created huge problems with chloride impurities. Cubic structures of sodium chloride quickly crystallized and inhibited the formation of titanium dioxide NPs on top of the glass substrates. The sodium impurities originated from the quartz glass tube that was employed as the reactor. At temperatures above  $400^\circ\text{C}$ , sodium impurity ions percolated from the quartz tube reactor, which caused sample contamination and inhibited growth of titanium dioxide nanostructures on top of the glass substrates. Hence, **Figure 1** shows a scanning electron microscopy (SEM) micrograph of cubic sodium chloride crystals on top of fluorine glass substrates.

Due to sodium ion impurity, it was necessary to select and design a tube reactor that could withstand deposition temperatures above  $400^\circ\text{C}$  and at the same time does not introduce any impurity elements to titanium dioxide nanoparticles. Secondly, titanium tetrachloride fumes at high temperatures are highly toxic, acidic, and have fast diffusion rates. The developed fumes were highly acidic and mobile at elevated temperatures. The fumes produced corroded all rubber tubing, seals, and O rings fitted on the USP system which caused serious carrier gas leakage problems. Thirdly, a dense cloud of titanium chloride fumes that formed during the deposition process further inhibited the growth of titanium dioxide nanostructures. As a result, it was difficult to deposit thin films of sufficient thickness ( $10\ \mu\text{m}$ ). This was due to low aerosol containing the titanium precursor volumes as compared to the amount of titanium tetrachloride vapors. In addition, titanium chloride in the presence of hydrous ethanol solvent was easily hydrated to form titanium hydroxide which precipitates inside the pneumatic nebulizer; this inhibited the nebulization process as the precursor quickly precipitated inside the nebulizer. This made it very difficult to atomize the precursor solution. Also, atomization of large particulates of  $\text{TiO}_2$  hydroxides led to the development of large nano-agglomerates inside the thin film structure of amorphous  $\text{TiO}_2$  phase inside the anatase  $\text{TiO}_2$  thin film which is not desirable in developing thin films for photovoltaic applications. Furthermore, there was non-uniform deposition of  $\text{TiO}_2$  thin films as some areas on the substrate were found to be thicker than others and other areas contained no  $\text{TiO}_2$  nanoparticles at all, as shown in **Figure 2**. Hence, due to corrosive nature of the titanium chloride precursor, toxicity, and ease

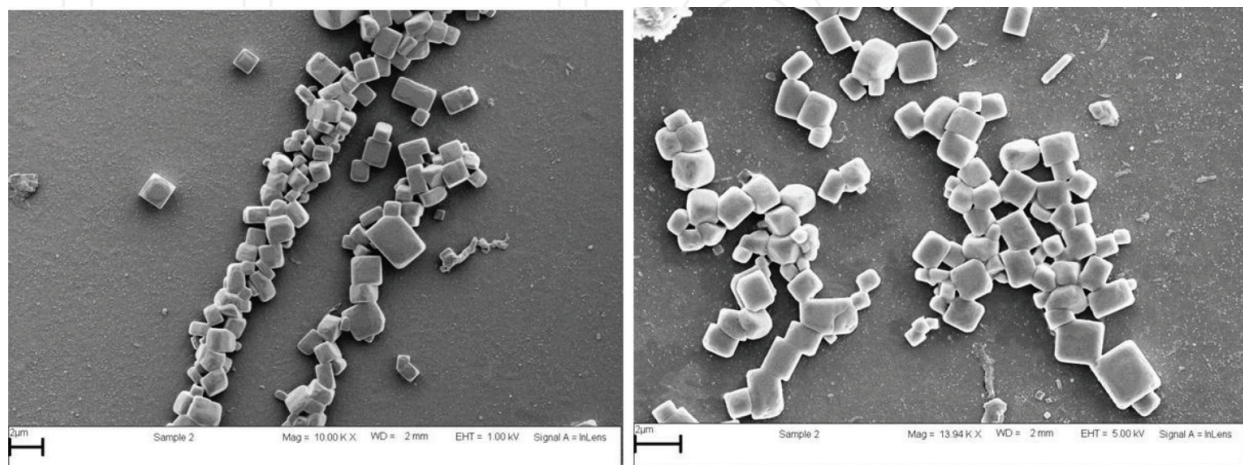


**Figure 1.** An SEM image showing NaCl cubic crystals that were formed on fluorine-doped tin oxide glass substrate.

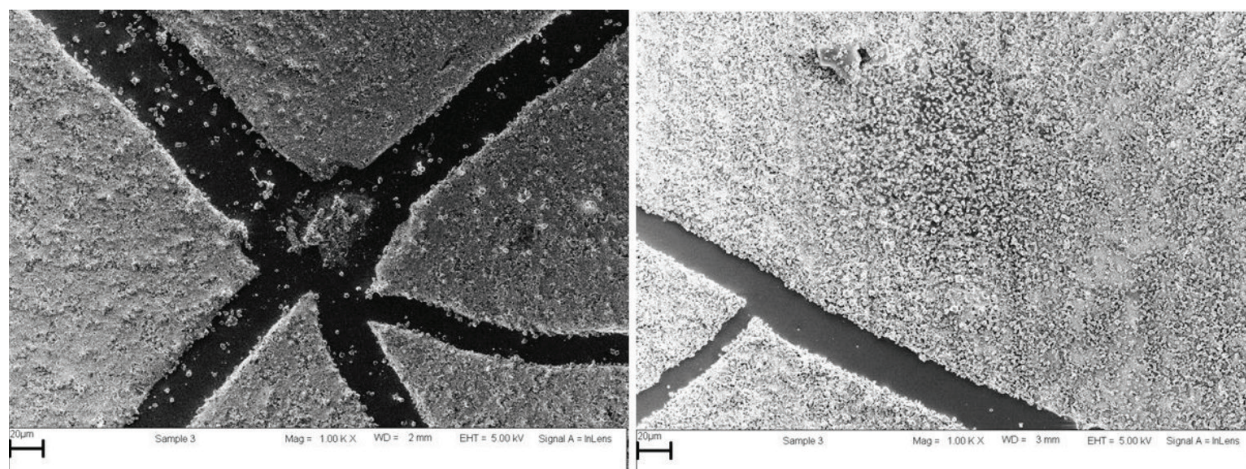


**Figure 2.** An SEM image of non-uniformly coated TiO<sub>2</sub> thin film.

at which titanium chloride precursor precipitates, when selecting a precursor for SP, it was deemed necessary to avoid chloride precursors of titanium.

### 1.1.2. Substrate geometry

It was also discovered that only some areas of the substrate facing the aerosol flow were fully coated. Areas on the substrate downward the aerosol flow were partially coated due to substrate orientation. The deposited thin films had cracks in them due to sudden temperature drop when the system was turned off. Fourthly, it took several hours for the system to cool down to room temperature. Fifthly, the round tube furnace employed had poor heat insulation. Hence, after some hours of operation, the temperature of the laboratory could rise to as far 38°C, which made monitoring of the spray pyrolysis deposition very difficult. Furthermore, it was impossible to mount such a spray pyrolysis system directly to a normal laboratory workbench as this presented a higher fire risk. In addition, all rubber tubings and O rings could not withstand high temperatures as they needed to be constantly replaced. This posed a further health risk due to leakage of argon and titanium precursor vapors into the working environment. Lastly, there was no way of regulating the relative humidity, and the relative humidity on rainy or overcast days (humidity up to 65%) made spraying impossible due to the formation of white TiO<sub>2</sub> hydroxides in the precursor solution. This made it very difficult to atomize the precursor solution.

## 2. USP operational conditions

### 2.1. Safety

The system should be enclosed so that it can safely operate on a standard laboratory bench. It also needs to have exhaust facilities into a sufficiently ventilated area. There was also a need to replace the tube furnace with a split tube furnace that had heat guides on. This made

it easy and safe to operate with aluminum tubing and/or quartz tubes as reaction vessels. The furnace was built in such a way that no heat should be dissipated into the work environment. It was also desirable to discontinue the use of titanium tetrachloride as a precursor. Titanium iso-propoxide and titanium (IV) butoxide were also more attractive to use as precursors since these are safe, non-toxic liquids, and obviate the need for expensive gas handling systems.

## 2.2. Geometry control

The other problem that needed urgent attention was the issue of substrate orientation. It was discovered that disposition of thin films at an oblique angle of  $30^\circ$  or with substrate lying on the floor of the quartz tube caused inhomogeneous thin film coating. We designed an aluminum substrate holder that secured the substrate at  $90^\circ$  of the reaction vessel axis, facing the incoming aerosol flow. Aluminum was chosen as the metal of choice because it's stable at deposition temperatures of  $400\text{--}500^\circ\text{C}$ , and it is a good conductor of heat. It also allowed pre-heating of substrates prior to thin film deposition. In addition, significant fluctuations in the temperature at about  $400^\circ\text{C}$  could result in the  $\text{TiO}_2$  film having a mixed amorphous-Anatase phase. Naturally, this outcome is undesirable.

## 2.3. Deposition area

Dye sensitized solar cells consist of an active area for instance titanium dioxide NPs deposited and the rest of the area on fluorine doped tin oxide (FTO) glass substrate is used for solar cell contacts. It was desirable that the substrate be masked; this allowed production of a thin film area of  $0.5\text{ cm}^2$ , which is desirable for dye solar cell applications. To achieve accurate control of the film thickness, the system was calibrated to produce sufficient thin films in deposition times of 20–30 min.

## 2.4. Relative humidity

Excess humidity will result in  $\text{TiO}_2$  particulates sticking to the deposited film. In SP spray deposition, it is always desirable to have adjustable and repeatable humidity control. It was anticipated that mixtures of dry nitrogen ( $\text{N}_2$ ) and wet nitrogen ( $\text{N}_2 + \text{H}_2\text{O}$ ) could be fed into the system in order to control the relative humidity. However, this proved to be costly, and we opted to use the carrier gas, argon, to provide dry environment with success.

## 3. The spray pyrolysis system

Following the operational design considerations as has been discussed in Section 2, a novel USP system was designed and constructed specifically for production of anatase  $\text{TiO}_2$  nanostructures and thin films for solar cell applications. **Figure 3** presents a graphic diagram of the USP system that was optimized for deposition of  $\text{TiO}_2$  NPs and TFs.

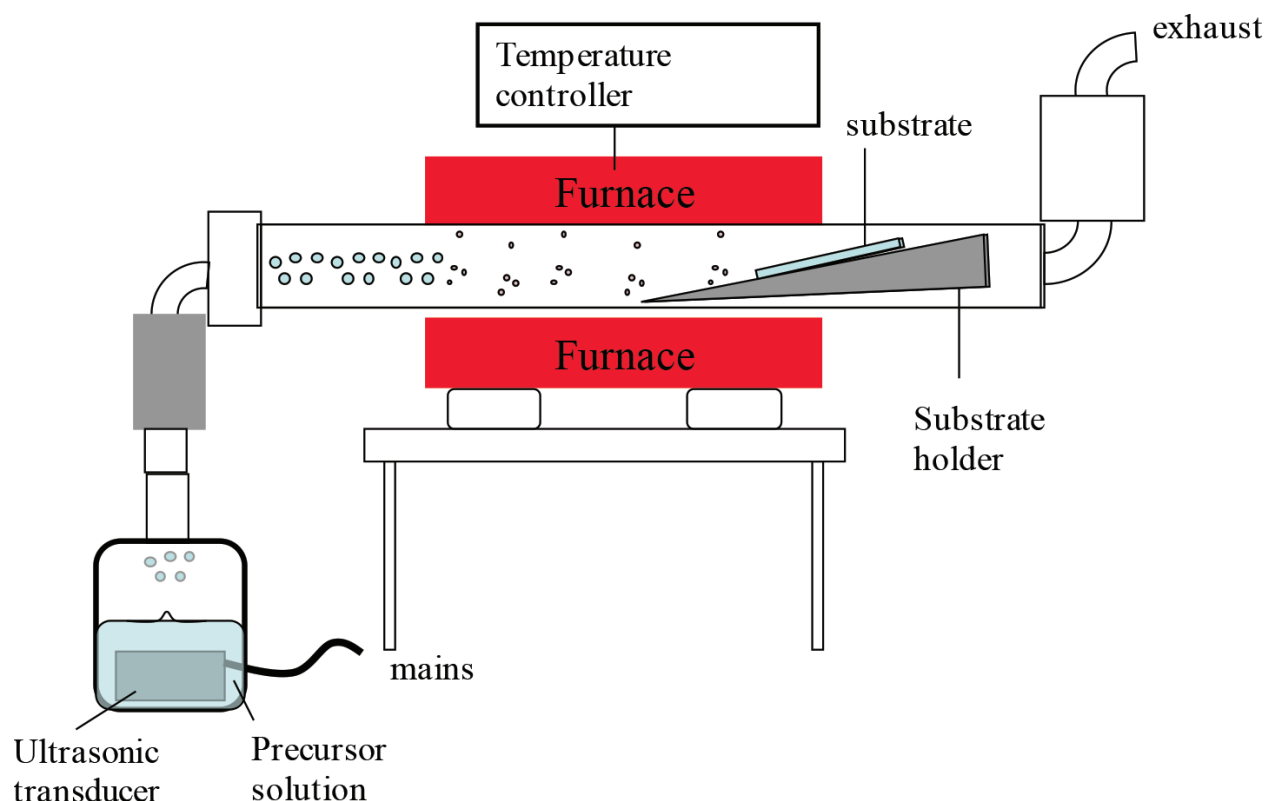


Figure 3. A graphic diagram of the USP system.

The design of a USP system comprises an (1) ultrasonic chamber, a (2) carrier gas system, (3) a heated zone or furnace with a temperature control unit, (4) substrate holder, and (5) exhaust system. The ultrasonic chamber houses a transducer, producing ultrasound waves at a frequency of 1.67 MHz that were focused to the precursor solution to produce vapors of ultrasound droplets. The argon carrier gas system was used to deliver the precursor droplets into the reaction zone that was either quartz or aluminum tube at a constant flow rate of 6 ml/min. The quartz or aluminum tube was in a temperature-controllable furnace with the substrate holder placed perpendicular to the direction of gas flow inside the tube. Both deposition temperatures and flow rate influenced the shape, morphology, and crystalline structure of the TiO<sub>2</sub> NPs and TFs. These TiO<sub>2</sub> layers were deposited on commercial viable substrates.

### 3.1. Selection of TiO<sub>2</sub> precursor

Use of titanium (IV) sulfate and titanium (IV) chloride precursor solutions has been reported [16]. Fabrication of TiO<sub>2</sub> NPs and TFs with titanium (IV) sulfate has been reported to have mixed crystalline phases of TiO<sub>2</sub>. It has been reported that use of titanium (IV) sulfate always resulted in uncontrolled formation of various phases of TiO<sub>2</sub> due to nature of preparation method, with the amorphous phase being dominant in the dried samples. While use of titanium (IV) chloride solution resulted in formation of an undesirable rutile phase for solar cell applications, use of titanium (IV) phosphate precursors has resulted in formation of uncontrolled mixtures of anatase and rutile phases in the annealed TiO<sub>2</sub> NPs and TFs. It has been

reported that the amorphous phase of  $\text{TiO}_2$  preexisted prior to formation of the crystalline phases, even in situations where the produced NPs/TFs had rutile as the main dominant phase. In this regard, it is imperative to select the appropriate precursor for use in SP system. Proper choice of a precursor is a primary issue in material synthesis. Titanium iso-propoxide, also known as tetraisopropyl titanate (TPT), was chosen as the  $\text{TiO}_2$  precursor. Apart from being the most commonly used precursor in the literature, this titanium alkoxide is also used in many solar cell production lines. Titanium tetrachloride/titanium (IV) chloride ( $\text{TiCl}_4$ ) is another common  $\text{TiO}_2$  precursor, which results in chlorine contamination [16]. In addition, its corrosive by-products (HCl) are produced in the reaction. It has been reported in literature that levels can be high enough to prevent nanomaterial crystallization on FTO glass substrates and can also cause thin film or poor film adhesion onto the substrate [16]. In any case, the level of contamination observed with titanium iso-propoxide is much smaller than with titanium (IV) chloride. Also, it has been reported that the use of titanium (IV) chloride results in formation in rutile and anatase phase mixtures, [17] and we also discovered that the use of titanium butoxide resulted in the formation of 95% of the anatase phase. In this work, titanium iso-propoxide and titanium butoxide were used as the precursors for the synthesis of  $\text{TiO}_2$  NPs and TFs.

In addition, these precursors have the following added advantages:

1. They are non-corrosive and non-toxic, listed as being mild skin and eye irritants.
2. They can be highly purified and have an almost indefinite shelf life.
3. As a liquid, they are relatively easy to handle, although they should not be exposed to a naked flame. The fact that it is not dangerous makes the addition of titanium iso-propoxide system a relatively easy and safe task as no special gas handling equipment is required.
4. They are very volatile at low temperatures ( $50^\circ\text{C}$ ), which means that they will be readily decomposed.
5. They can be ultrasonically sprayed directly without dilution.
6. It has been observed that there is enough oxygen in the titanium iso-propoxide molecule that the reaction to form  $\text{TiO}_2$  can proceed without additional oxygen in the ambient.

### 3.2. Pyrolysis of $\text{TiO}_2$ solutions

Countless processes take place concurrently before a vapor droplet forms solid nanostructures on the substrate. When the ultrasonically generated precursor vapor droplet hits the surface of the substrate, formation of solid nanostructures proceeds by evaporation of solvent molecules, decomposition of the metal salt, and spreading of the droplet. Numerous mechanisms have been presented for pyrolysis that lead to formation of solid-phase nanoparticles and thin films in spray pyrolysis. The route for each of these theories is entirely dependent on nature of the precursor solution and the experimental conditions the ultrasonically generated precursor solution is exposed to. The mechanism of the reaction of titanium iso-propoxide

aerosol to form TiO<sub>2</sub> depends on the droplet size. When the majority of the ultrasonically generated vapor droplets hits the surface of the preheated glass substrates, depending on the experimental conditions inside the reactor such as pressure, temperature, humidity, and stoichiometry composition of the precursor droplet, smaller droplets normally burst under pressure and decompose into solid NPs. However, due to collision between the precursor droplets due to random gaseous motion, some smaller droplets tend to coalesce to form bigger vapor droplets. The bigger droplets tend to decompose into solid NPs on the surface of the preheated substrates. However, pyrolysis of precursor droplets in spray pyrolysis occurs in much the same way as chemical vapor deposition systems, which apply to all aerosol processes. **Figure 4** presents the proposed aerosol droplet transport, decomposition, and deposition on substrate at various temperatures in spray pyrolysis.

In process A, the decomposition rate at very low temperatures (< 100°C) will be slower than the deposition rate, and a liquid film will form on the surface. This layer will slowly dry; however, it will still contain many organics and probably cracks. At this stage, titanium dioxide will be present as hydrated white hydroxide and in its amorphous phase. As the temperature of the substrate increases in process B, the solvent from the droplets evaporates during its flight before reaching the surface, and a precipitate strikes the substrate where decomposition occurs. In process C, the solid precipitate melts and vaporizes (or sublimates), and the vapor diffuses to the substrate and undergoes a reaction there. This corresponds to true CVD. At higher temperatures (process D), the vapor undergoes a chemical reaction before impinging upon the substrate. The droplets in the aerosol have formed solid particles that stick to the surface of the substrate. Titanium iso-propoxide pyrolyses at temperatures greater than 350°C and films deposited in this method at 450–600°C are considerably harder than films produced by colloidal synthesis methods.

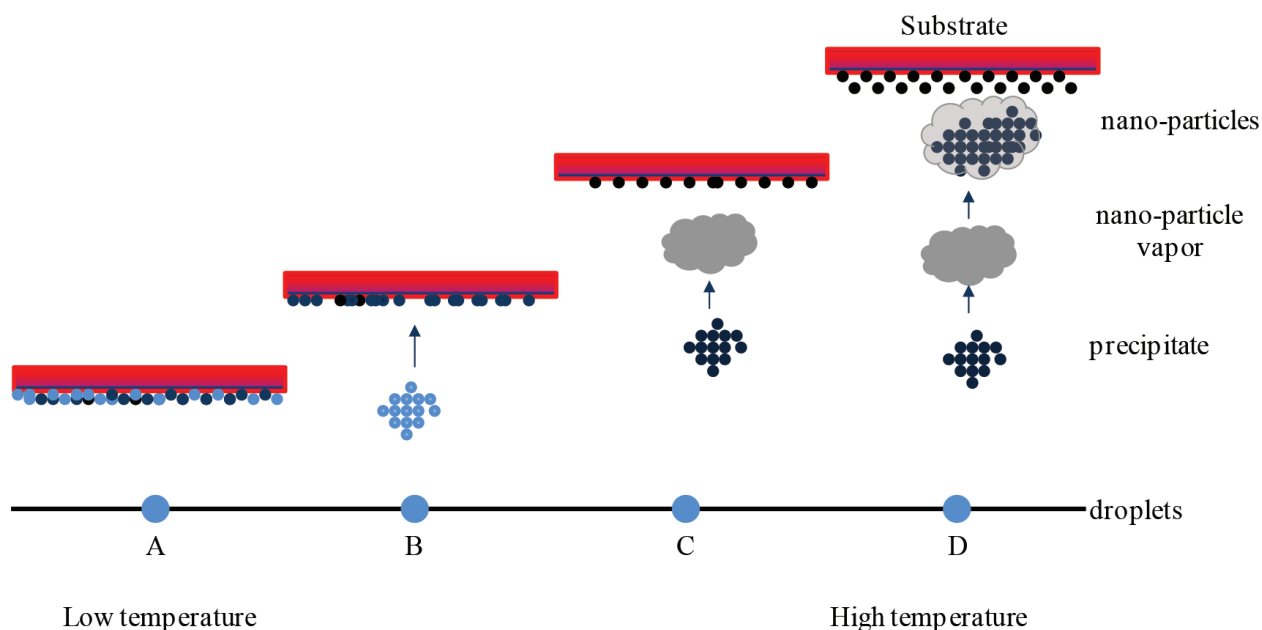
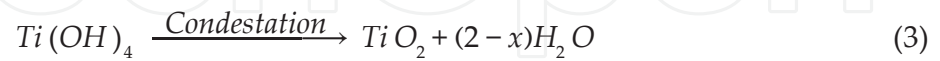
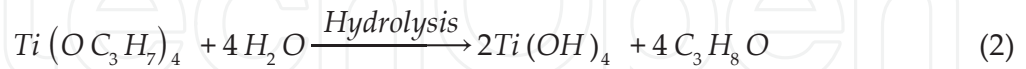


**Figure 4.** Illustrations of aerosol droplet transport, decomposition, and deposition on the substrate at various temperatures.

In inert and dry argon environment and assuming the absence of water vapor, the decomposition of titanium iso-propoxide occurs via pyrolysis to form  $TiO_2$  and proceeds as follows:



However, such an assumption is very dangerous as there are various sources of water vapor, for instance, the solvent ethanol, the carrier gas, and the spray pyrolysis vessel itself. There is, to some extent, formation of titanium dioxide via a hydrolysis process which is governed by Eq. (1).



One should note that the formation of titanium dioxide occurs to a large extent by Eq. (1) and to a negligible extent by Eqs. (2, 3 and 4). The size and shape of the deposited titanium dioxide NPs are determined by the molar ratio of adsorbed water in Eq. (3), that is  $(x = [H_2O])/[Ti]$ . At  $x < 10$ , relatively spherical, monodisperse particles are formed. On the other hand, at values of  $x > 10$ , particles formed are unstable precipitates, and this results in aggregates which form a state dispersion of colloidal nanoparticles (sol-gel) with sizes larger than 100 nm.

n is the process responsible for the formation of stable dispersion of colloidal particles in dispersion medium. In other words, it may be defined as a process of converting a precipitate into colloidal solution by shaking it with dispersion medium in the presence of a small amount of electrolyte.

#### 4. Design considerations and optimization of USP system

The design of the current spray pyrolysis system, the knowledge gathered in the Section 4, and Section 5 were used as guidelines to design the new system. Section 6 presents the desirable system designs and parameters taken into consideration.

##### 4.1. Sizing of ultrasonic reaction vessel

The Bernoulli's theorem of conservation of energy of fluid flow in channels of varying cross-sectional areas was considered useful in deriving the relationship between droplet size and volume it occupied. This theorem was also applied here in determining the proper volume to house the ultrasonic nebulizer. This is mainly because the volume of the reaction vessel plays a vital role in defining the final NPs crystallite size. The Bernoulli's theorem states that:

$$p + \frac{1}{2} \rho v^2 + \rho gy = \text{constant.} \quad (5)$$

For a droplet distribution of mass ( $m$ ) moving at mean speed ( $v$ ), and occupying a volume ( $V$ ) under pressure ( $P$ ), the chain rule for  $P = mV$  substitution results in

$$dp + \left[ \frac{1}{2} m v^2 + mgy \right] dV + pvdv + g\rho dy = 0 \quad (6)$$

and assuming small variations in the droplet size change with change in velocity, which is typical in materials deposition processes,  $dv$  is approximately equal to 0. Eq. (6) then reduces to

$$dp = -EdV - g\rho dy \quad (7)$$

where  $E$  is the total energy of the droplet. If the droplet diameter is introduced into this equation, it is possible to rewrite Eq. 7 as

$$\frac{dD}{dp} = -\frac{dD}{EdV + g\rho dy} \quad (8)$$

Therefore, at a constant position  $y$ ,

$$\frac{dD}{d\rho} = -\frac{dD}{EdV} \quad (9)$$

Similarly, at a constant volume of the system but varying position,

$$\frac{dD}{dp} = -\frac{dD}{g\rho dy} \quad (10)$$

The theoretical data models have shown a sharp increase of droplet sizes with change in USP system volume. **Figure 5** shows the experimental evidence of droplet diameter dependence of USP volume which is in mutual agreement with theoretical models. This effect of volume change has also been observed by droplets generated by Mwakikunga *et al.*, [10, 20, 21].

The main goal for this work was to develop an ultrasonic spray pyrolysis system capable of realizing nano-sized powders, and considering previous findings by Mwakikunga *et al.*, [20, 21]. An ultrasonic reaction system with maximum volume of 0.1 m<sup>3</sup> was developed. **Figure 6** shows the USP reaction vessel used in this chapter. The quartz glass used for the vessel provided a non-corrosive environment for housing the acidic precursors of TiO<sub>2</sub>.

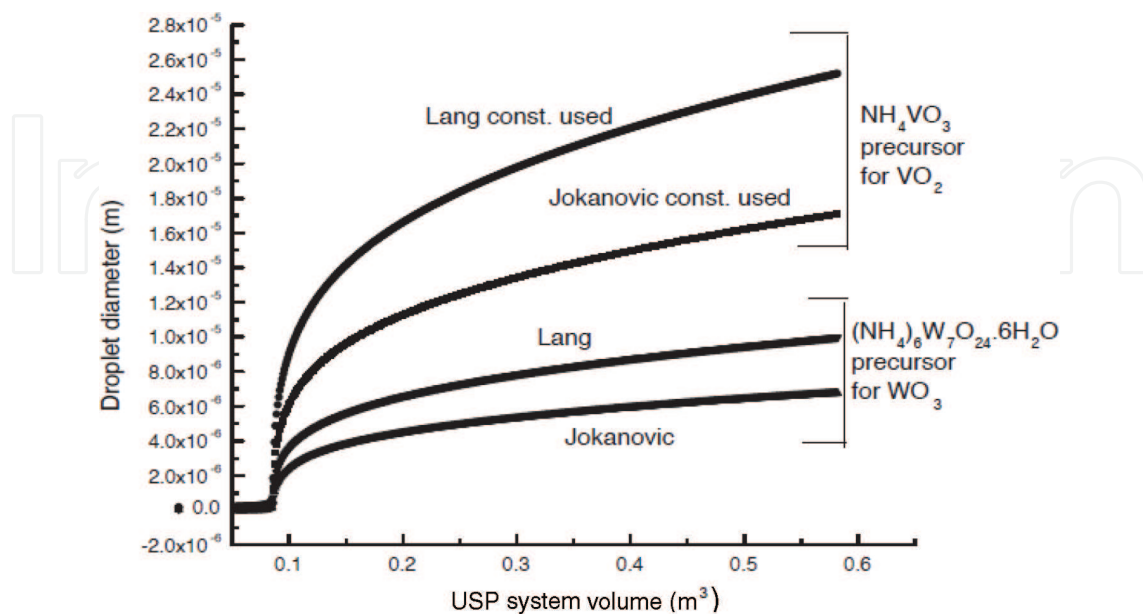


**Figure 5.** Experimental evidence of droplet diameter dependence on USP system volume [10, 20].

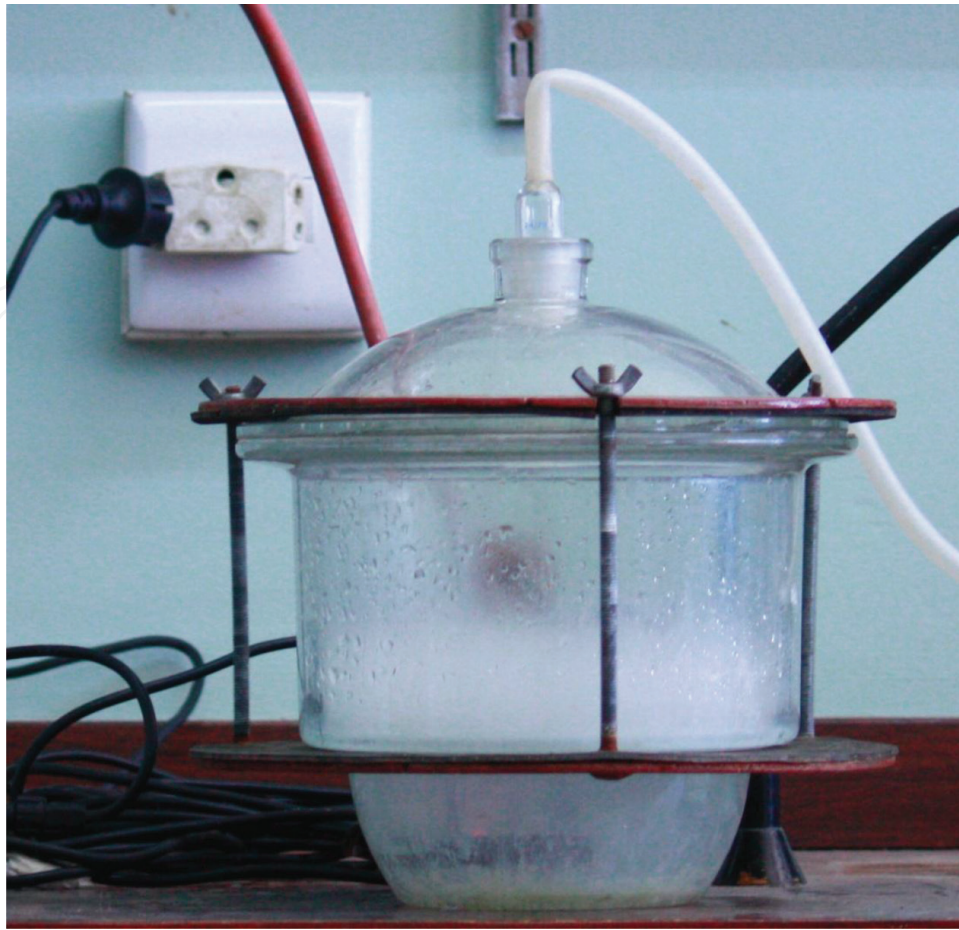


**Figure 6.** An actual photograph of the USP reaction vessel used.

#### **4.2. Selection of ultrasonic nebulizers**

Ultrasonic nebulizers used in this project were purchased from Time-to-Digital Converter (TDC) power products Co. Ltd, Germany. The ultrasonic nebulizer employed composed between three and five piezoelectric transducers driven at frequency of 1.7 and 4.8 MHz, each driven by a dedicated ultrasonic generator. There were several reasons for selecting an ultrasonic nebulizer, rather than pneumatic nebulizers. Firstly, pneumatic nebulizers require high pressurized gas systems that are either from a compressor or gas tank. This inherent property would increase the initial production cost of titanium dioxide. This meant that the designed system would require sophisticated equipment to control the gas flow rates, pressure regulator, high pressure valves, and tubing. We therefore preferred a nebulizer that could operate at standard atmospheric pressures. Secondly, it was believed that with proper control of nebulizer operation frequency, the reaction mechanism for droplet generation would be tuned to behave similar to a belt furnace atmospheric pressure chemical vapor deposition (APCVD) system used in the PV industry. Thirdly, there is a huge potential in scaling the project to industrial scale for fabrication of dye solar cell, considering the ease of assembly and the need for low operation skills. In addition, the ultrasonic nebulizer housing is manufactured from titanium alloy and stainless steel housing. The titanium alloy was chosen mainly because of

its high mechanical durability, excellent ability to resist conversion of vibrational energy into heat (hence it does not heat up the precursor during material deposition), and high chemical resistance toward most titanium alkoxide precursors which are highly acidic. **Figure 7** shows the nebulizers used in the chapter.

After some trial runs, we discovered that the 4.8 MHz nebulizer would be unsuitable for our application shown in (b) of **Figure 7**. This was due to the extremely high volume of aerosol produced [ $(300 \times 7) \pm 50$  cc/hr] which also caused high flow rates. The resulting titanium dioxide deposited thin films on the FTO glass substrates that were too thick. Titanium dioxide yields were just too high and uncontrollable. It was also suspected that due to the high flow aerosol rates and short residence times of the aerosol inside the heating zone of the furnace, amorphous phase of titanium dioxide was formed. We therefore opted to use the 1.7 MHz nebulizer to synthesize titanium dioxide thin films. We discovered that with controlled flow rates of 6 ml/min, we could deposit a thin film which was approximately 10  $\mu$ m. To achieve longer deposition times, the lowest flow rates had to be used. Although a fine mist often emerged from the nozzle, the low volumes being pumped were not sufficient to create a cloud of droplets of several inches in diameter. Occasionally, the nebulizer would also “stall” and produce high volumes of aerosol which would cause deposition of liquid vapor onto the substrate. This resulted in high agglomerates of TiO<sub>2</sub> nanoparticles being incorporated into the film. These defects reduced the chemical resistance and produced high electrical resistance on carbon-doped titanium films, which were undesirable for dye solar cell applications. We therefore resorted to carry out thin deposition with



**Figure 7.** Ultrasonic nebulizers employed in the study: (a) shows the 1.7 MHz ultrasonic nebulizer with power supply unit and (b) shows the 4.8 MHz ultrasonic nebulizer with power supply unit.

30 min spray breaks. Spray deposition using the 1.7 MHz nebulizer over the 4.8 MHz ultrasonic nebulizer poised several advantages:

1. The 1.7 MHz nozzle enabled use of very low flow rates of almost  $2 \times 10^{-2}$  ml/min, which increased the residence time of the aerosol vapor inside the heating zone. This gave enough time for complete pyrolysis/hydrolysis of titanium dioxide precursors to anatase phase of titanium dioxide.
2. The use of low flow rate gives allowance for achieving, with high success, well-controlled, consistent repeatable thin films. This setup resulted in thin film deposition times at 450°C of 25–30 min.
3. In addition, the power required by 1.7 MHz ultrasonic nebulizer required from the ultrasonic generator to atomize titanium dioxide precursors was in the order of 2.5 W. **Table 1** shows the specifications of the nebulizers chosen.

#### 4.3. Selection of the spray reactor

NPs and TFs can be deposited by wet chemistry methods [2] as well as by solid state techniques that vaporize the precursor to a gaseous phase [3, 9–12]. Use of techniques that employ an intermediate gas phase prior to formation of NPs and TFs presents numerous merits as compared to the wet chemistry methods since the purification, drying, and annealing procedures are dismissed. As techniques that employ a gaseous phase duck, the intermediate purification procedures employ high liquid volumes of expensive, corrosive, toxic, and unpleasant solvents and/or surfactants prior to formation of final high-purity NPs and TFs. Liquid phase techniques have low throughput due to losses of NPs during the purification process. Spray pyrolysis reactors that have been modernized for fabrication of nanopowders consist of flame reactors [5], furnace reactors [10, 11], and plasma reactors. Use of techniques that are assisted by a gaseous phase intermediate, it is possible produce all sorts of wide band gap semiconductors as NPs and TF, giving potential for new or low

	1.7 MHz ultrasonic nebulizer	4.8 MHz ultrasonic nebulizer	Test condition 1.7 MHz nebulizer	Test condition 4.8 MHz nebulizer
Resonant frequency	1.7 MHz $\pm$ 0.1 MHz	4.8 MHz $\pm$ 0.1 MHz		
Resonant impedance	5 $\Omega$ max.	3 $\Omega$ Max.		
Static capacitance	1400 pF $\pm$ 15%	2400 pF $\pm$ 15%		
Mist output	(300 $\times$ 3) $\pm$ 50 ml/hr	(300 $\times$ 7) $\pm$ 50 ml/hr	Precursor temperature of 25°C and precursor level of 38 mm	Precursor temperature of 25°C and precursor level of 38 mm
Life time	5000 hr/min	5000 hr/min		
Power in put	2.5 W	6.5 W	Standard circuit pin	Standard circuit pin

**Table 1.** Specifications of the 1.7 MHz ultrasonic nebulizer and 4.8 MHz ultrasonic nebulizer.

cost-efficient applications. The specific gaseous phase techniques fluctuate on how thermal energy is transferred to the precursor vapors to eliminate the solvent molecules. They also differ on how the precursor solution is transported to the reaction site, and financial aspects, final product quality, and characteristics do affect the choice of spray reactor. Currently, the PV industry employs spray pyrolysis systems with flame reactors for the production of NPs and TFs. However, use of vapor flame reactor system is restricted by choice of metal precursors. Moreover, it is not easy to deposit multi-component semiconductor NPs and TFs with consistent chemical stoichiometry. This is due to the differences in the chemical reaction rates and pressures of the reactants. Spray pyrolysis systems are equipped with tubular reactors such as a furnace, and each ultrasonically vaporized vapor molecule contains the same atomic ratios of the precursor solutions [10, 11]. The produced micro-droplets in actual fact serve as a discrete micro-reactor. This is an advantage of aerosol vapor-assisted phase as compared to flame reactors, where the stoichiometry of each of the precursor solution is not the same. This is a major advantage since in vapor flame reactors, several reactants have to be vaporized simultaneously with special care to obtain the desired stoichiometry. Furthermore, flame reactor systems are costly in operational costs and the quality of the final product in either stoichiometry or crystalline morphology leaves a lot to be desired. Spray pyrolysis systems that use furnace reactors offer superior quality at low operational cost and minimum operator skill.

Spray-assisted methods for deposition of NPs and TFs differ by how the thermal energy is delivered to the generated aerosol vapors to facilitate solidification of NPs and TFs and, at the same time, facilitating solvent evaporation. **Figure 8** presents key spray methods discussed in this work, namely spray pyrolysis in a tubular reactor (SP) [10], spray pyrolysis using a vapor flame reactor (VFSP), the emulsion combustion method (ECM), [16] and flame spray pyrolysis (FSP). In fact, in all the spray techniques presented in **Figure 8**, the precursor is generated in much the same way and vaporizes into a mist of droplets. These spray techniques reveal a significant difference in how the thermal energy is delivered to generated mist of the precursor to facilitate solidification and solvent evaporation. Additionally, the difference is also in the energy source that facilitates formation of NPs and TFs—such as in VFSP, a liquid fuel is needed to ignite the reaction. Reactors with an independent source of energy supply are not affected by the nature of the selected titanium dioxide precursors and solvents. Double distilled water is often preferred as the aqueous solvent in systems with an external energy supply due to financial advantages, ease of handling, and the outstanding solubility for metallic salts. Spray systems which have an internally supplied source of power and fuel to facilitate solvent evaporation and eventual solidification of NPs and TFs present numerous disadvantages. Mainly due to the nature of the different combustion rates of the precursor solution, there are different temperature gradients with the same reactor and large temperature differences, which in turn result in different solidification rates of the NPs and TFs. This results in differences in the crystalline morphology of the deposited TFs and NPs. In addition, flame spray pyrolysis has higher operation cost as compared to other methods. The triumph of fabricating practical metal oxides, mixed-metal oxides, and metals on metal oxides from inexpensive precursors in an inexpensive aerosol process revolutionized the design of spray pyrolysis reactors.

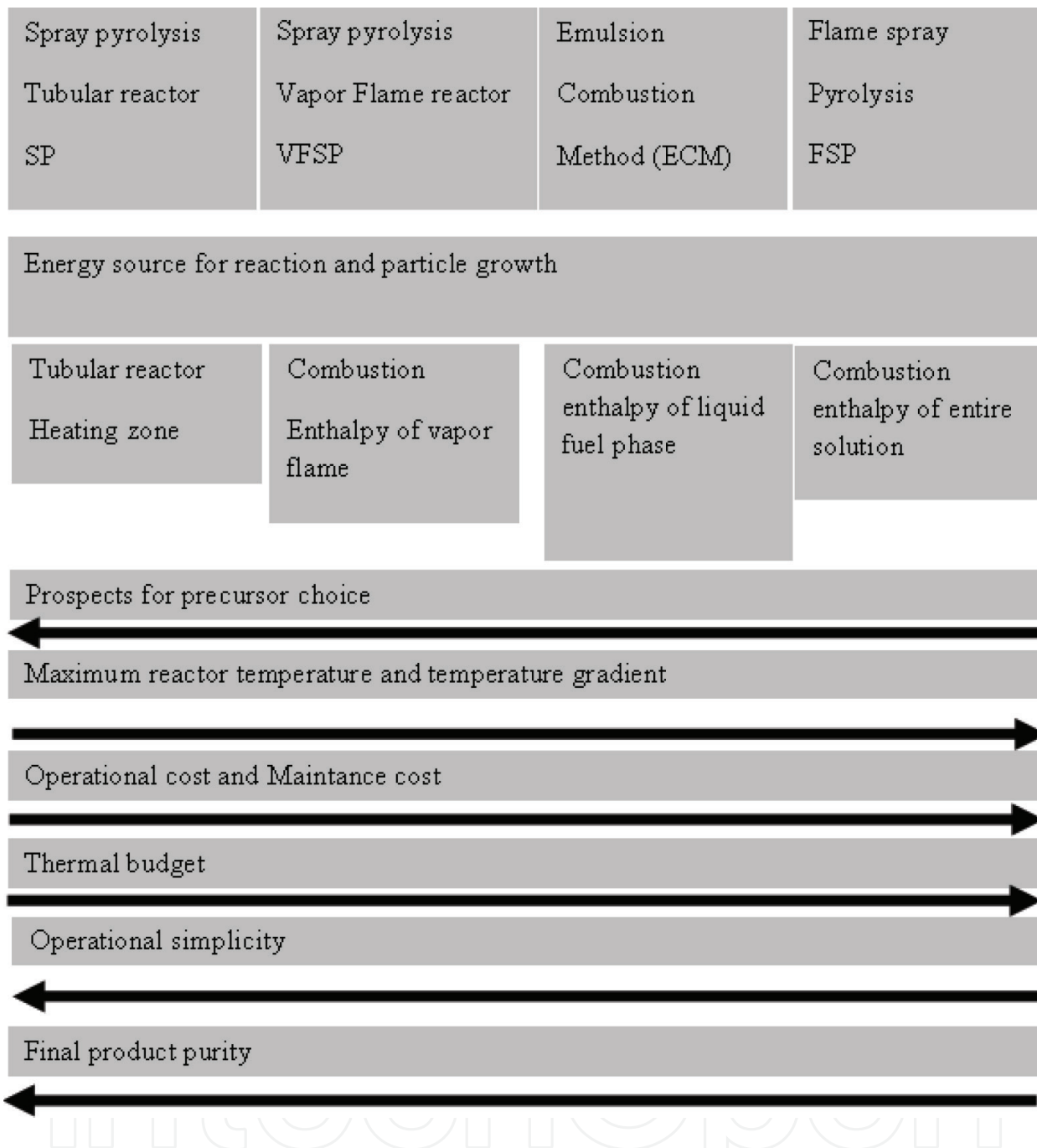


**Figure 8.** Main spray methods operated at ambient pressure for gas phase-assisted NPs deposition from metal precursors. Precursors are transported within a solvent into a reaction zone, where reaction and the final product formation occurs.

Spray pyrolysis systems, with reactors that employ thermal energy from the element of a coil, provide a uniform and controlled form of heat energy to evaporate solvent molecules and, at the same time, facilitate solidification of NPs and TFs of controlled consistent crystallinity, morphology, and stoichiometry as compared to other techniques. Moreover, spray pyrolysis systems that employ furnace reactors present several advantages such as (1) operational simplicity, (2) minimum throughput (in terms of consumables), (3) lower thermal budget, and (4) lower operational cost. Moreover, there is no need for subsequent heat treatment after deposition of either the NPs or TFs. Furthermore, tubular reactor systems offer the opportunity of

industrial scaling. These inherent advantages were some of the drivers of the choice of the tubular reactor used at Fort Hare shown here in **Figure 9**, and **Figure 10** shows the actual aluminum reactor used in the study. **Figure 10 (a)** shows the aluminum reactor for production of thin films **(b)** production of nano-particles. Compared to liquid-phase precipitation methods, flame reactors and laser ablation systems powders produced by spray pyrolysis systems employing furnace reactors are beneficial since the deposited NPs have consistent chemical composition, consistent crystalline phase, are of high purity, and rarely require several heat treatments after deposition [8].

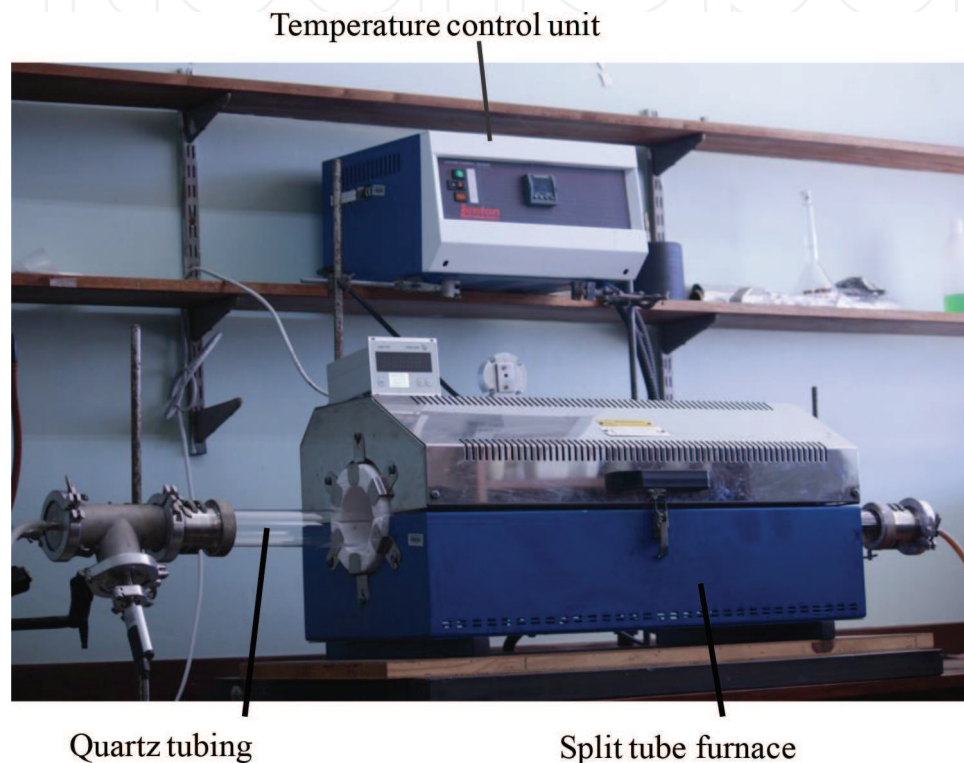


**Figure 9.** Shows the actual photograph of the split tube furnace employed in the synthesis of TiO<sub>2</sub> nano structure in the study.



**Figure 10.** The aluminum reaction vessels used for ultrasonic spray pyrolysis deposition of TiO<sub>2</sub> NPs and TFs.

In addition, spray pyrolysis methods offer excellent spatial mixing of the precursor molecules and are capable of depositing functional multi-component semiconductor oxides.

#### 4.4. Design of the substrate holder

The novelty of our USP system originates from the angle at which the substrate interacts with the incoming aerosol vapor as shown in **Figure 11**. Most systems that have been utilized employ a substrate holder with the substrate vertically parallel to the incoming aerosol beam. In our USP system, the substrate holder and hence the substrate are perpendicular to the aerosol stream as shown in the schematic representation of **Figure 12**. **Figure 11**, shows the aluminum substrate holder employed in the study.

The choice of the deposition angle  $\theta = 0^\circ$  can be best explained by considering schematics in **Figure 13**. **Figure 13** shows that the aerosol vapor stream is incident at an angle  $\theta$  with the normal to the substrate surface. **Figure 13(a)** shows a schematic of the setup and **Figure 13(b)** shows a corresponding vector diagram. The glancing angle deposition (GLAD) technique is the extension of the commonly used oblique angle deposition (OAD) in thin film deposition industry. The experimental setup for the oblique angle deposition is shown here in **Figure 13**. In most ideal cases, the aerosol vapor stream has an incident angle,  $\theta$ , with the respect to the normal substrate surface.

At a glancing angle deposition  $\theta$ , the substrate interacts with the stream of the precursor equally from the vertical and lateral directions. Hence, at this angle  $\theta$  of deposition, growth of NPs results in randomly formed islands on the surface of the substrate.

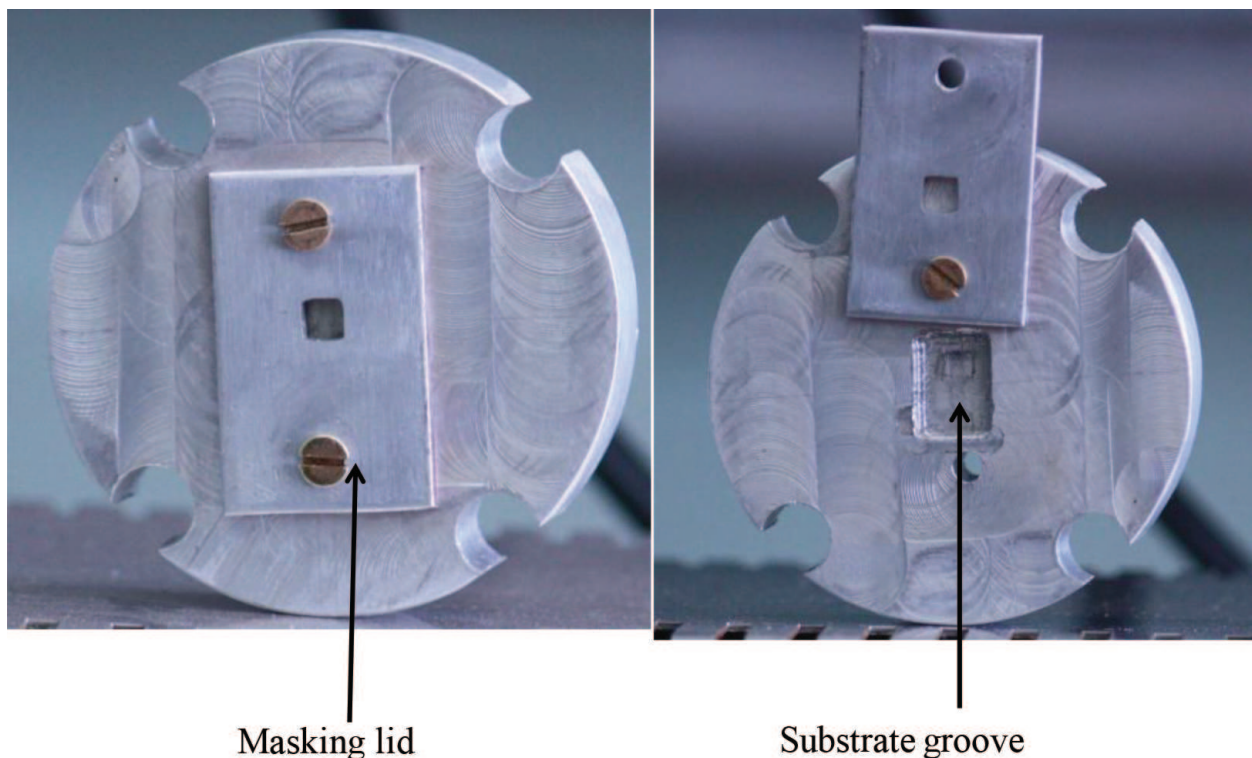


**Figure 11.** The aluminium substrate holder employed in open and closed configuration.

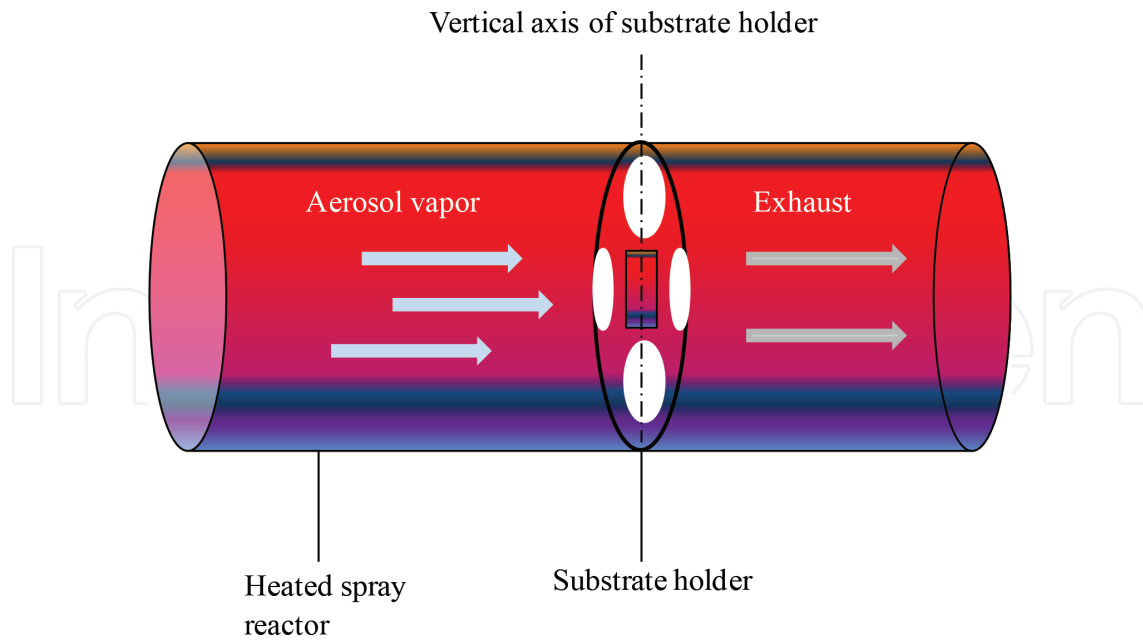


**Figure 12.** Schematic presentation of substrate holder orientation in the spray reactor.

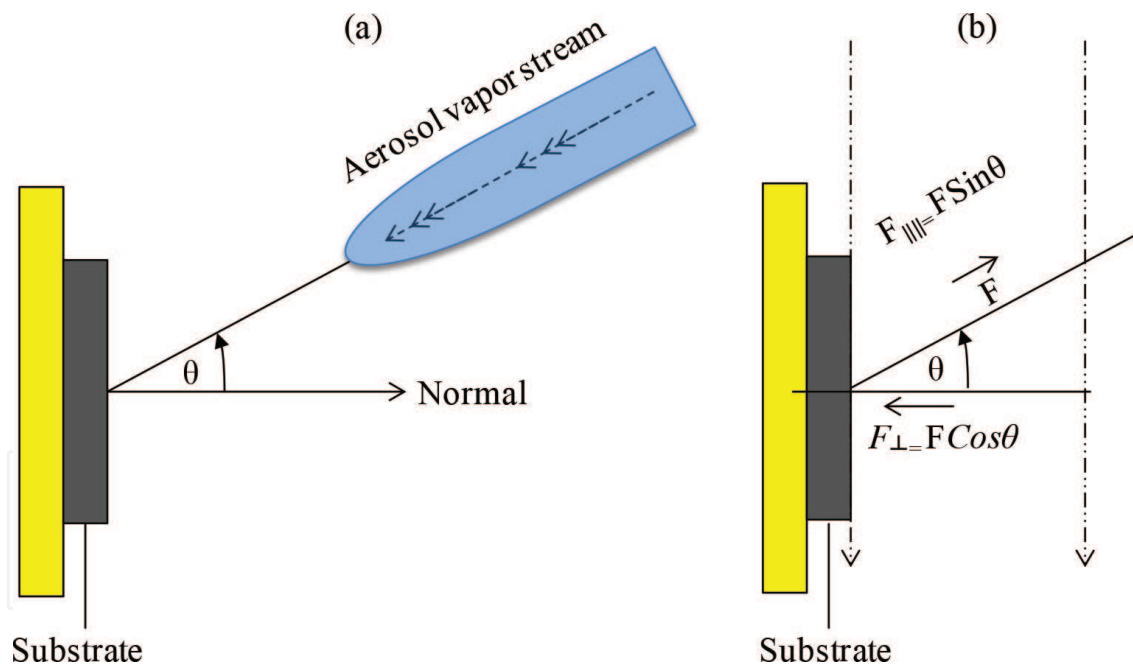


**Figure 13.** (a) A schematic drawing for the experimental setup for oblique angle deposition and (b) the incident aerosol vapor stream  $F$  can be decomposed into different components:  $F_{\perp}$  is perpendicular to substrate and  $F_{\parallel}$  is parallel to the substrate.

deposition continues, the initially formed and nucleated islands of NPs will act as shadowing centers. Hence, all of the tallest nanoparticle islands will expand into columns at the expense of other areas on the substrate that don't receive the aerosol vapor stream. Vector diagram in **Figure 13(b)** shows that the lateral component  $F_{\parallel}$  is the source revealing the enhanced shadowing effect. For the oblique angle deposition, since  $F_{\parallel}$  remains constant during spray

deposition, a columnar film with angle  $\beta$  will be formed. Through scanning electron micrograph analysis, Hawkeye *et al.* [22] have shown that the shift of angle  $\theta$  in deposition of silicon thin films had tremendous effects on the geometrical arrangement of the deposited NPs. They found that at  $\theta = 30^\circ$ , small columns of silicon began to grow, at  $\theta = 60^\circ$ , the columnar structures of silicon became obvious, and at  $\theta = 80^\circ$ , the columnar structures of silicon become more pronounced. They have also reported that at  $\theta = 0^\circ$ , where the incoming aerosol vapor stream was not affected by lateral component of the vector  $\mathbf{F}$  in **Figure 13** (hence the growth of NPs and TFs was not affected by the shadowing effect), continuous and uniform nano-TFs were deposited as shown here in **Figure 13**. We therefore adopted this idea when designing the substrate holder for our horizontally orientated ultrasonic spray pyrolysis system as well as the aluminum reaction chamber that is capable of supporting the substrate in a vertical position. Thin film deposition was done at  $\theta = 0^\circ$  for the development of nanostructures for photovoltaic applications. **Figure 14** shows the preliminary results that were obtained with the substrate holder in this configuration.

One can observe that the developed titanium dioxide TFs by this methodology were mesoporous and have spherical NPs, which have mesoporous nanostructure morphology for dye solar cells.

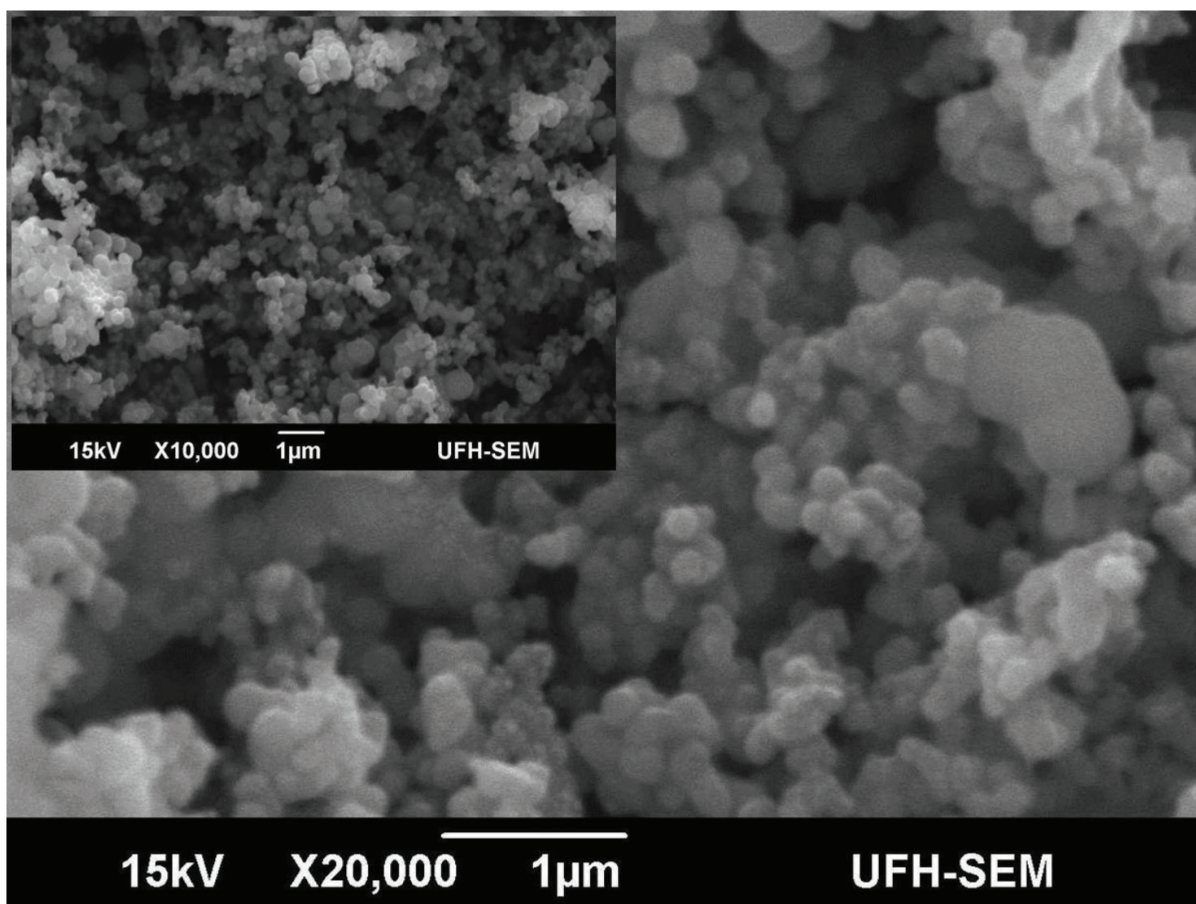


**Figure 14.** SEM micrographs showing effects of the titanium dioxide thin film produced at  $\theta = 0^\circ$ , with an insert showing the same sample on a different spot and on a lower magnification.

## 5. Operation of the ultrasonic spray system

In its final form shown in **Figure 15**, the ultrasonic spray system incorporated all of the above component as well as those listed in Section 5. **Table 2** outlines the standard deposition parameters for the precursors chosen. The gas flow rates were optimized in order to extend thin film coverage in the forward direction. At lower flow rates of 1–2 ml/min, ultrasonic spray depositions were performed at the lowest system operating temperature of 450°C; this is mainly because of high-enough residence times spent by aerosol vapor droplets inside the heating zone. At higher flow rates of 5–6 ml/min, system operating temperature was increased to a maximum value of 500°C to accommodate the short residence times spent by the aerosol vapor droplets. Throughout this whole project, argon was used as the only carrier gas. Also, the aluminum substrate holder was used in most cases for thin film synthesis.

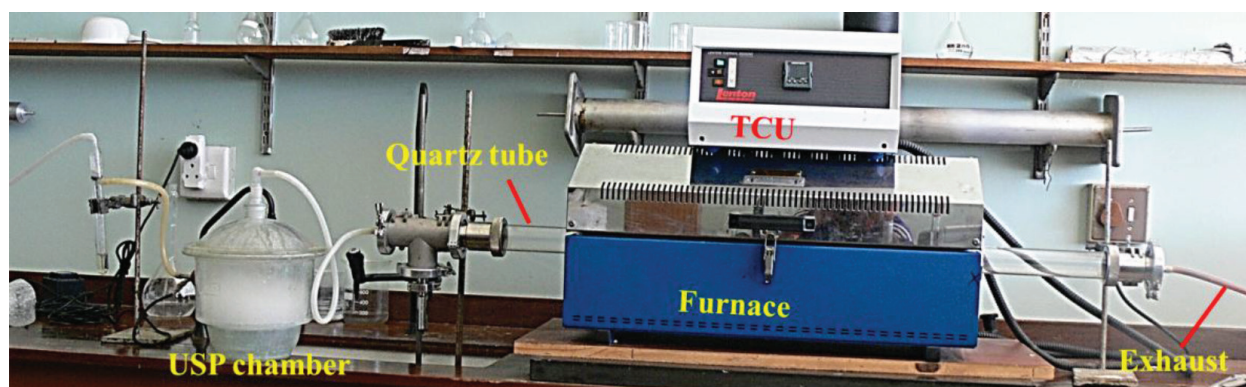


**Figure 15.** USP system in its final form.

Process parameters	Ultrasonic spray pyrolysis	
	@ 450°C	@ 500°C
Argon flow rate	1–2 ml/min	5–6 ml/min
Ultrasonic vessel pressure (Atm)	1	1
Precursor temperature (°C)	25	25
Precursor pH	1.95	1.95
Substrate type & temperature (°C)	FTO Glass & 450°C	FTO Glass & 550°C
Deposition time (m)	120	30
Deposition Angle (°)	0	0
Annealing temperature (°C)	450	450

**Table 2.** Showing operation conditions for USP system.

## 6. Results and discussions

### 6.1. SEM analysis

**Figure 16** presents SEM micrographs of the undoped and N-TiO<sub>2</sub> NPs synthesized by ultrasonic spray pyrolysis technique with different levels of nitrogen doping. SEM images, both undoped and N-TiO<sub>2</sub> NPs, reveal the formation of spherical-shaped TiO<sub>2</sub> NPs. Moreover, the SEM micrographs reveal that the surface morphology and shape of both undoped and N-TiO<sub>2</sub> NPs change as the nitrogen dopant level increases. All thin films formed were mesoporous and had a multiparous network structure. Furthermore, the presence of Ti, N, and O in our PSP samples has confirmed the successful pyrolysis of our Ti precursors. Moreover, there are trace levels of Al that might have originated from the Al substrate holder or aluminum reactor that was used in the study, and they were no other contaminants detected from elemental analysis [10, 11].

**Figure 17** shows the XRD spectra of the USP-fabricated TiO<sub>2</sub> samples. XRD analysis has that the USP-fabricated undoped and N-TiO<sub>2</sub> NPs have an anatase polymorph with peaks at

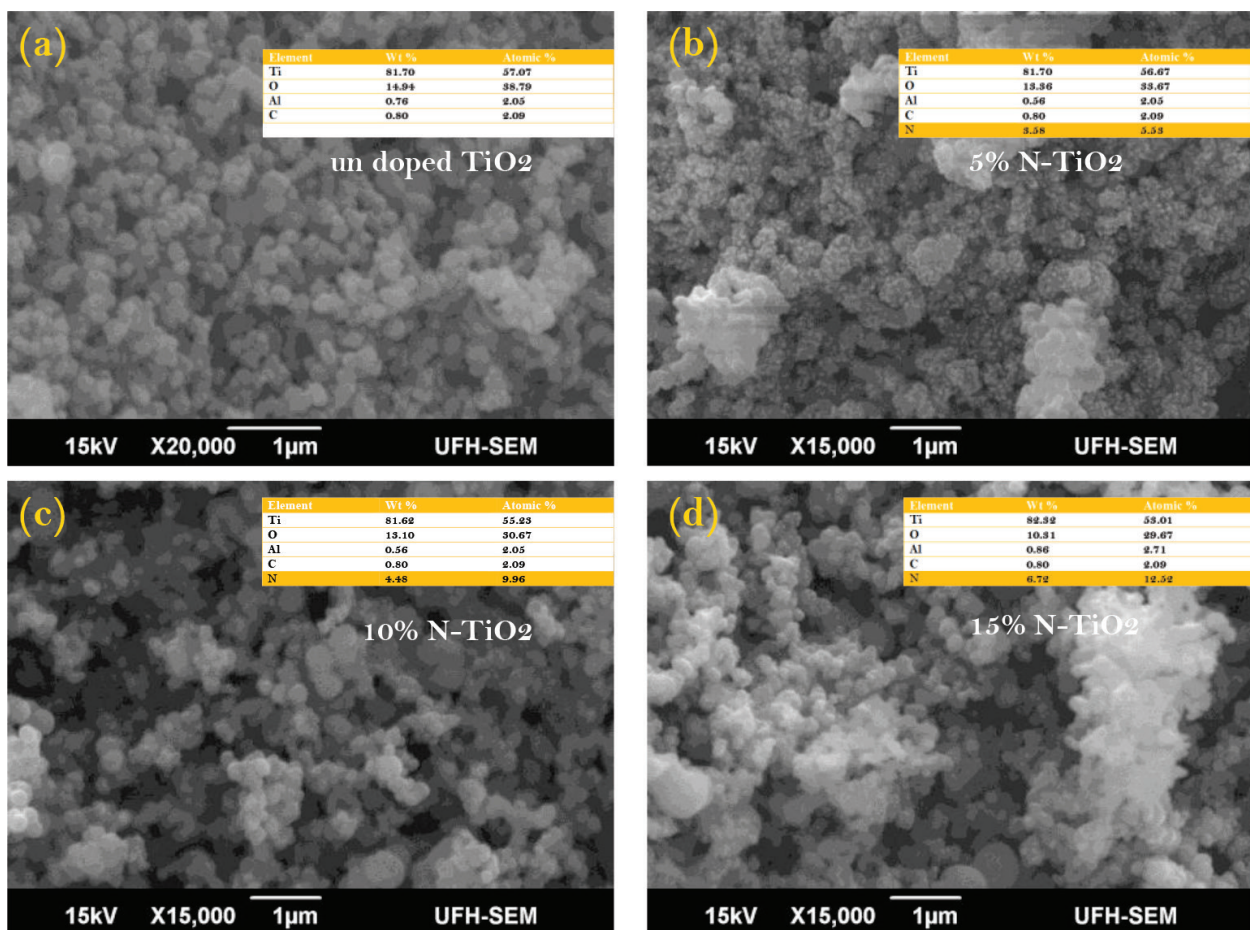


**Figure 16.** Shows SEM micrographs of (a) undoped TiO<sub>2</sub> (b) 5% of N-TiO<sub>2</sub> samples, (c) 10% of N-TiO<sub>2</sub> samples, and (d) 15% of N-TiO<sub>2</sub> samples. Additionally, insert in (a), (b), (c), and (d) reveal the elemental composition analysis by EDX of the undoped TiO<sub>2</sub> and N-TiO<sub>2</sub> samples respectively.

2 $\theta$  angles and [hkl] planes of 25.67° [101], 38.19° [004], 48.56° [200], 53.91° [105], 63.14° [204], 68.98° [116], 70.72° [220], and 75.65° [215]. Moreover, close inspection of the dominant peak with 2 $\theta$  angles of 25.67° has shown a peak shift to higher 2 $\theta$  values, which is indicative of substitutional nitrogen doping. The crystallize size was calculated using Scherrer's equation  $t = 0.9\lambda/\beta\cos\theta$  where  $\lambda$  is wavelength of X-ray in Å and  $\beta$  is full width at half maximum in

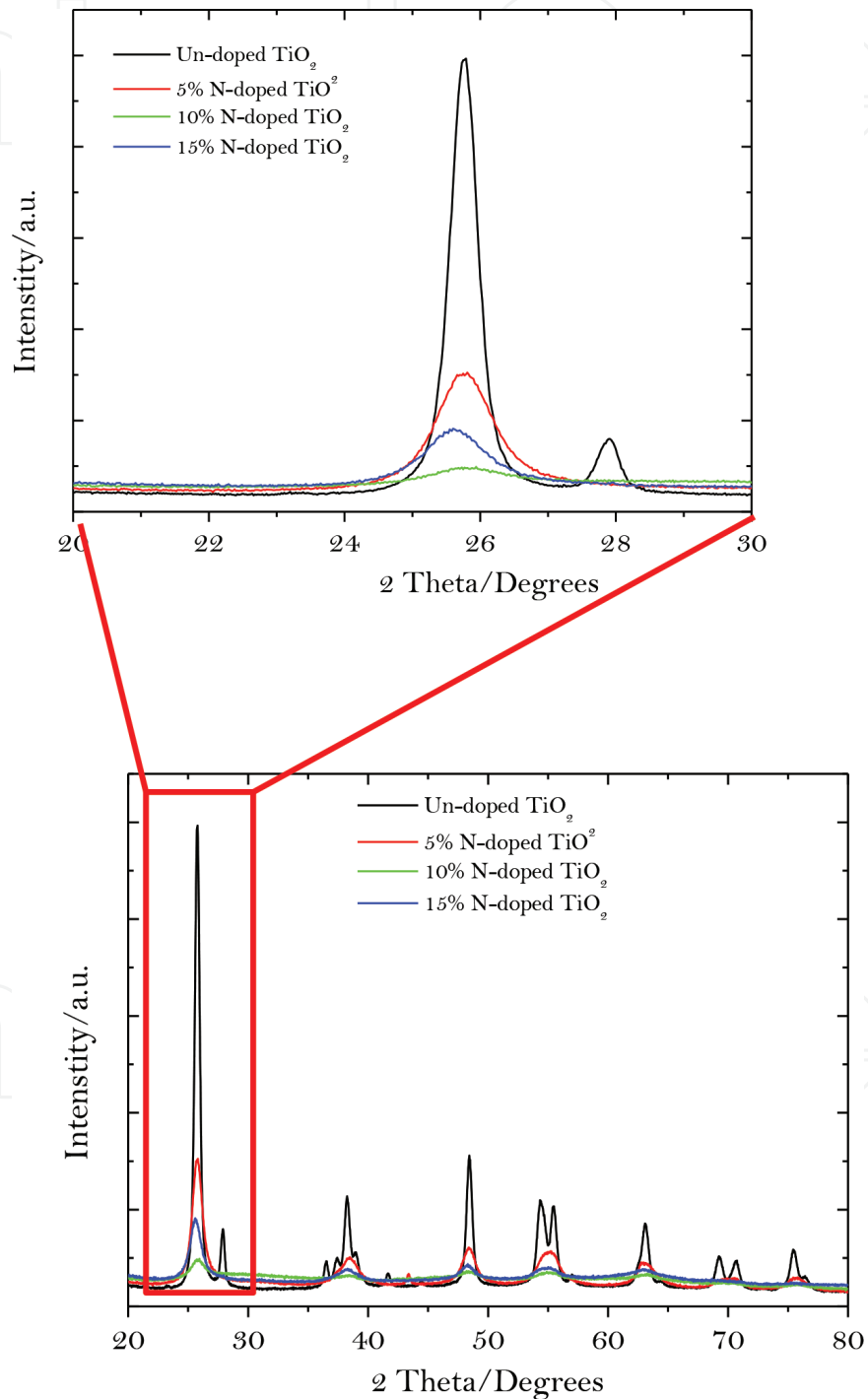


**Figure 17.** X-ray diffraction (XRD) spectra of the USP-fabricated TiO<sub>2</sub> NPs.

radian. The USP-fabricated undoped and N-doped TiO<sub>2</sub> NPs had nanoparticle sizes of 23.12 nm, 24.15 nm, 26.2 nm, and 25.9 nm for undoped, 5% N-TiO<sub>2</sub>, 10% N-doped TiO<sub>2</sub>, and 15% N-doped TiO<sub>2</sub>, respectively.

## 6.2. Raman spectroscopy analysis

Raman spectroscopy (RS) has revealed that the TiO<sub>2</sub> samples shown in **Figure 18** have Raman active bands characteristic of anatase phase at 153.43 cm<sup>-1</sup>, 209.9 cm<sup>-1</sup>, 401.7 cm<sup>-1</sup>, 517.6 cm<sup>-1</sup>, and 641.9 cm<sup>-1</sup> with symmetries of E<sub>g</sub>, E<sub>g</sub>, B<sub>1g</sub>, A<sub>1g</sub>, B<sub>1g</sub>, and E<sub>g</sub>, which is in mutual agreement with XRD analysis [10].

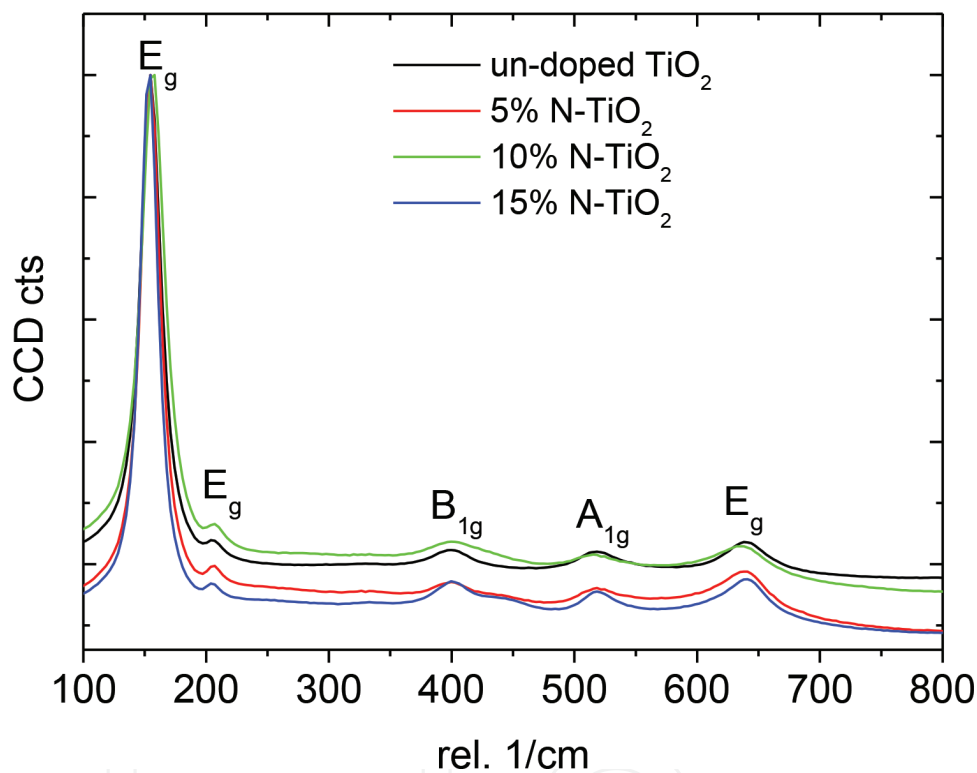


**Figure 18.** Raman spectra of the USP-fabricated samples.

## 7. Conclusions

A good understanding of basic TiO<sub>2</sub> material properties along with knowledge of previous experiences when working with TiO<sub>2</sub> spray deposition systems formed the necessary requirements for the design of the new USP spray deposition for TiO<sub>2</sub> thin films. Thin films were required to be dense and defect free, exhibit good thickness uniformity, possess a high refractive index and low optical absorption, and be semiconducting. Examination of deposition techniques described in the literature leads to the author designing a novel USP system. USP system developed offered unique features in material in synthesis of pure undoped TiO<sub>2</sub> and

carbon-doped TiO<sub>2</sub> thin films and nanostructures. Firstly, we employed a horizontal furnace reactor as a contrast to most vertical systems in literature. Secondly, the horizontal system offered several potential advantages for deposition of thin films without any shadowing effect observed in the glancing or oblique angle depositions employed in most CVD systems. We managed to deposit samples at 0°, which allows the aerosol beam-containing precursor vapor to interact directly with the substrate uniformly. Furthermore, this allowed the system to use low deposition rates and the ability to deposit for a wide range of thin films via this method using different liquid precursors. Many of the desired TiO<sub>2</sub> film properties were obtained from films deposited using the USP system. XRD analysis has revealed the presence of anatase polymorph with peaks at 2θ angles and [hkl] planes of 25.67° [101], 38.19° [004], 48.56° [200], 53.91° [105], 63.14° [204], 68.98° [116], 70.72° [220], and 75.65° [215]. Additional Raman spectroscopy analysis has confirmed the presence of an anatase polymorph with Raman vibrational frequencies and symmetries 153.43 cm<sup>-1</sup>(E<sub>g</sub>), 209.9 cm<sup>-1</sup>(E<sub>g</sub>), 401.7 cm<sup>-1</sup>(B1g), 517.6 cm<sup>-1</sup>(A1g), and 641.9 cm<sup>-1</sup> (Eg). SEM images, both undoped and N-TiO<sub>2</sub> NPs, reveal the formation of spherical-shaped TiO<sub>2</sub> NPs. Moreover, the SEM micrographs reveal that the surface morphology and shape of both undoped and N-TiO<sub>2</sub> NPs change as the nitrogen dopant level increase.

## Acknowledgements

We are grateful for financial support from our sponsors, South African National Research Foundation (NRF) and Govan Mbeki Research and Development Centre (GMRDC) of the University of Fort Hare. The authors would also like to acknowledge the DST/CSIR Nanotechnology Innovation Centre, National Centre for Nanostructured Materials, and CSIR characterization of the TiO<sub>2</sub> NPs.

## Author details

Raymond Taziwa<sup>1,2\*</sup> and Edson Meyer<sup>2</sup>

\*Address all correspondence to: rtaziwa@ufh.ac.za

1 Chemistry Department, University of Fort Hare, The Republic of South Africa

2 University of Fort Hare Institute of Technology, University of Fort Hare, The Republic of South Africa

## References

- [1] Shirke BS, Korake PV, Hankare PP, Bamane SR, Garadkar KM. Synthesis and characterization of pure anatase TiO<sub>2</sub> nanoparticles. *J Mater Sci Mater Electron*. 2011;**22**:821-824. doi:10.1007/s10854-01-0218-4.

- [2] Yabing Z, Li Z, Dongping D. Single-step hydrothermal synthesis of strontium titanate nanoparticles. *Ceramics International*. 2015;**41**:13516-13524.
- [3] Nolan MG, Pemble ME, Sheel DW, Yates HM. One step process for chemical vapour deposition of titanium dioxide thin films incorporating controlled structure nanoparticles. *Thin Solid Films*. 2006;**515**:1956-1962.
- [4] Momeni, MM, Ghayeb Y, Gheibee S. Silver nanoparticles decorated titanium dioxide-tungsten trioxide nanotube films with enhanced visible light photo catalytic activity. *Ceramics International*. 2017;**43**:564-570.
- [5] Yildirim Serdar, Yurddaskal Metin, Dikici Tuncay, Aritman Idil, Ertekin Kadriye, Celik Erdal. Structural and luminescence properties of undoped, Nd<sup>3+</sup> and Er<sup>3+</sup> doped TiO<sub>2</sub> nanoparticles synthesized by flame spray pyrolysis method. *Ceramics International*. 2016;**42**:10579-10586.
- [6] Cotalan N, Rak M, Bele M, Cör A, Muresan LM, Milošev I. Sol-gel synthesis, characterization and properties of TiO<sub>2</sub> and Ag-TiO<sub>2</sub> coatings on titanium substrate. *Surface & Coatings Technology*. 2016;**307**:790-799.
- [7] Hwang Heewon, Yoon Soyeon, Seok Jeessoo, Kim Kyungkon. Di(2-pyridyl)ketone stabilized titanium dioxide nanoparticles for the room temperature processed electron transporting layer in organic photovoltaics. *Organic Electronics*. 2016;**28**:281-286.
- [8] Chaturvedia Amita, Joshi MP, Monda P, Sinhab AK, Srivastava AK. Growth of anatase and rutile phase TiO<sub>2</sub> nanoparticles using pulsed laser ablation in liquid: influence of surfactant addition and ablation time variation. *Applied Surface Science*. 2017;**396**:303-309.
- [9] Liu Zhongwei, Chen Qiang, Wang Zhengduo, Yang Lizhen, Wang Chuanyue. Production of titanium dioxide powders by atmospheric pressure plasma jet. *Physics Procedia*. 2011;**18**:168-173.
- [10] Taziwa R, Sideras-Haddad E, Erasmus RM, Manikandan E, Mwakikunga BW. Effect of carbon modification on the electrical, structural, and optical properties of TiO<sub>2</sub> electrodes and their performance in lab scale dye-sensitized solar cells. *International Journal of Photo Energy*. 2012;**2012**:904323-904354.
- [11] Taziwa R, Meyer EL, Chinyama KG. Raman temperature dependence analysis of carbon doped titanium dioxide nano-particles synthesized by ultrasonic spray pyrolysis technique. *Journal of Material Science*. 2012, **47**:1531-1540. doi:10.1007/s10853011-5943.
- [12] Ishizuka Shinnosuke, Kimura Yuki, Yamazaki Tomoya. In situ FT-IR study on the homogeneous nucleation of nanoparticles of titanium oxides from highly supersaturated vapour. *Journal of Crystal Growth*. 2016;**450**:168-173.
- [13] Funakoshi Kunio, Nonami Toru. Influences of saturation ratios on crystallization of anatase titanium dioxide by a titanium alkoxide hydrolysis. *Ceramics International*. 2008;**34**:1637-1642.

- [14] Kolen'ko YV, Kovnir KA, Gavrilov AI, Garshev AV, Frantti J, Lebedev OI, Churagulov BR, Tendeloo GV, Yoshimura M. Hydrothermal synthesis and characterization of nanorods of various titanates and titanium dioxide. *J Phys Chem B*. 2006;**110**:4030-4038.
- [15] Ito S, Kitamura T, Wada Y, Yanagida S. Facile fabrication of mesoporous TiO<sub>2</sub> electrodes for dye solar cells chemical modification and repetitive coating. *Sol Energy Mater Sol Cells*. 2003;**76**:3-13.
- [16] Rincón ME, Gómez-Daza O, Corripio C, Orihuel A. Sensitization of screen-printed and spray-painted TiO<sub>2</sub> coatings by chemically deposited CdSe thin films. *Thin Solids Films*. 2001;**389**:91-98.
- [17] Wilska S. An X-ray diffraction study to determine the effect of the method of preparation on the crystal structure of TiO<sub>2</sub>. *Acta Chemica Scand*. 1958;**8**:1796-1801.
- [18] Hsiang Hsing-I, Lin Shih-Chung. Effects of aging on nanocrystalline anatase-to-rutile phase transformation kinetics. *Ceramics International*. 2008;**34**:557-561.
- [19] Priol L, Baudel P, Louste C, Romat H. Theoretical and experimental study (linear stability and Malvern granulometry) on electrified jets of diesel oil in atomization regime. *J Electrostatics*. 2005; **63**: 899-904.
- [20] Mwakikunga BW. Nano-size effects optical, structural and phononic properties of VO<sub>2</sub> and WO<sub>3</sub> by ultrasonic nebulizer spray pyrolysis technique dissertation. Republic of South Africa University of 109, Johannesburg.
- [21] Harra J, Nikkanen JP, Aromaa M, Suhonen H, Honkanen M, Salminen T, Heinonen S, Levänen E, Mäkelä JM. Gas phase synthesis of encapsulated iron oxide-titanium dioxide composite nanoparticles by spray pyrolysis, julkaisussa. *Powder Technology, Vuosikerta*. 2013;**243**:46-52.
- [22] Hawkeye MM, Brett MJ. Glancing angle deposition: fabrication, properties, and applications of micro- and nanostructured thin films. *Journal of Vacuum Science & Technology A. Vacuum, Surface and Films*. 2007;**25**:1317-1335.

IntechOpen

